Enhanced oxygen reduction kinetics of IT-SOFC cathode with

$PrBaCo_2O_{5+\delta}/Gd_{0.1}Ce_{0.9}O_{2-\delta}$ coherent interface

Yang Zhang [a], Leyu Shen [a], Yuhao Wang [c], Zhihong Du [a, b], Binze Zhang [a], Francesco Ciucci [c, d], Hailei Zhao [a, b]*

[a] School of Materials Science and Engineering, University of Science and Technology Beijing, Beijing 100083, China

[b] Beijing Municipal Key Lab for Advanced Energy Materials and Technologies, Beijing 100083, China

[c] Department of Mechanical and Aerospace Engineering, The Hong Kong University of Science and Technology, Hong Kong, China

[d] Department of Chemical and Biological Engineering, The Hong Kong University of Science and Technology, Hong Kong, China
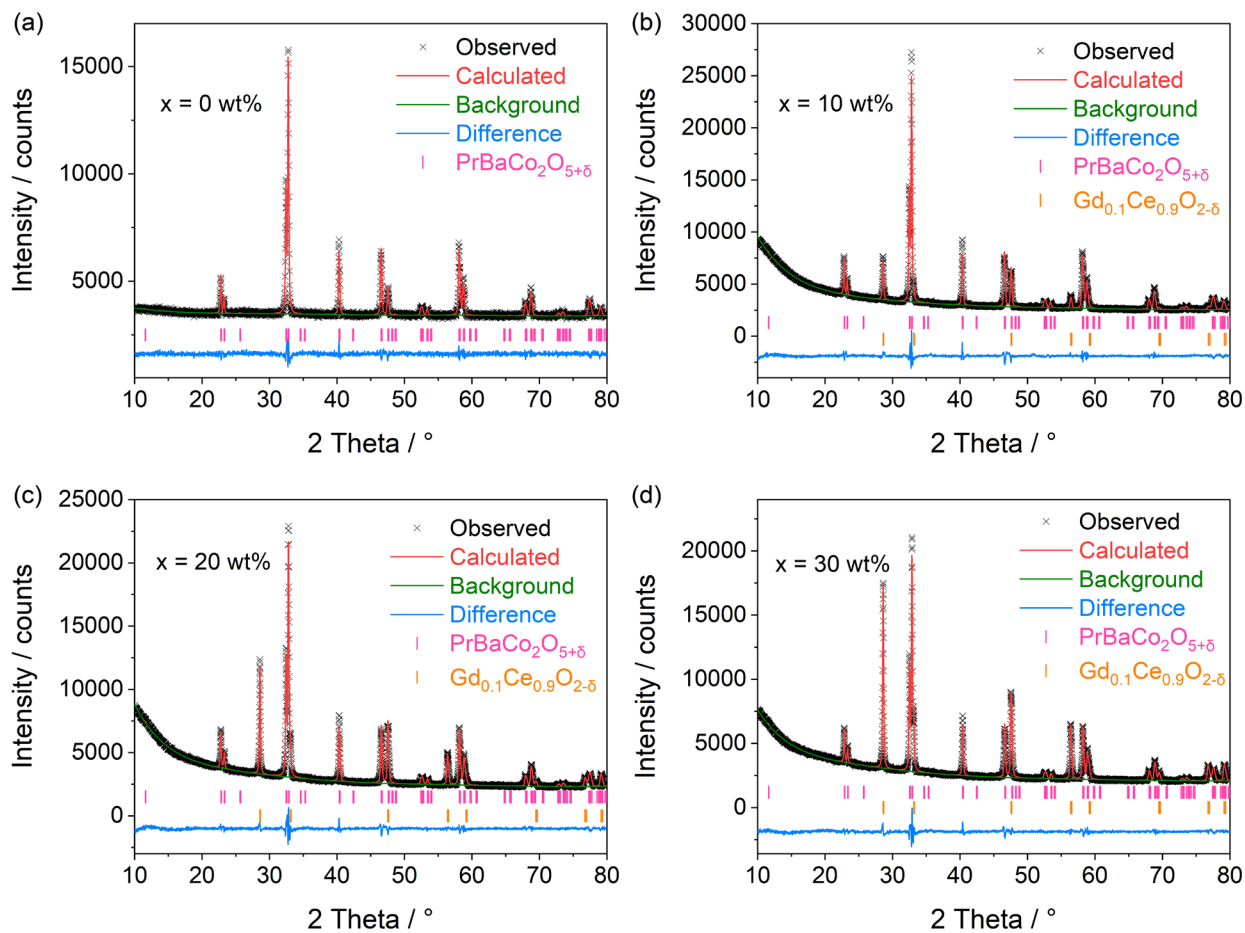
Supporting Information

Figure S1. Rietveld refinement for XRD patterns of samples PBC-xGDC, (a) x=0 wt%, (b) x=10 wt%, (c) x=20 wt% and (d) x=30 wt%.
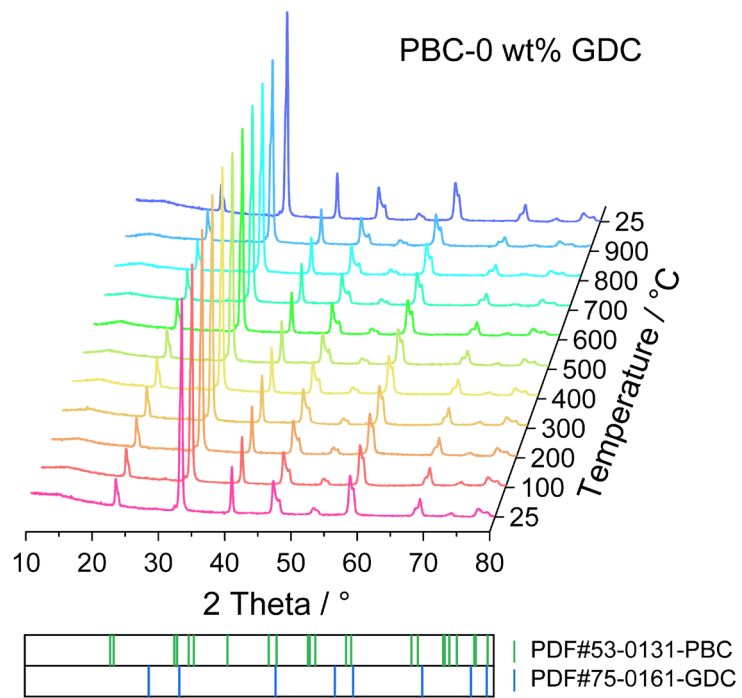
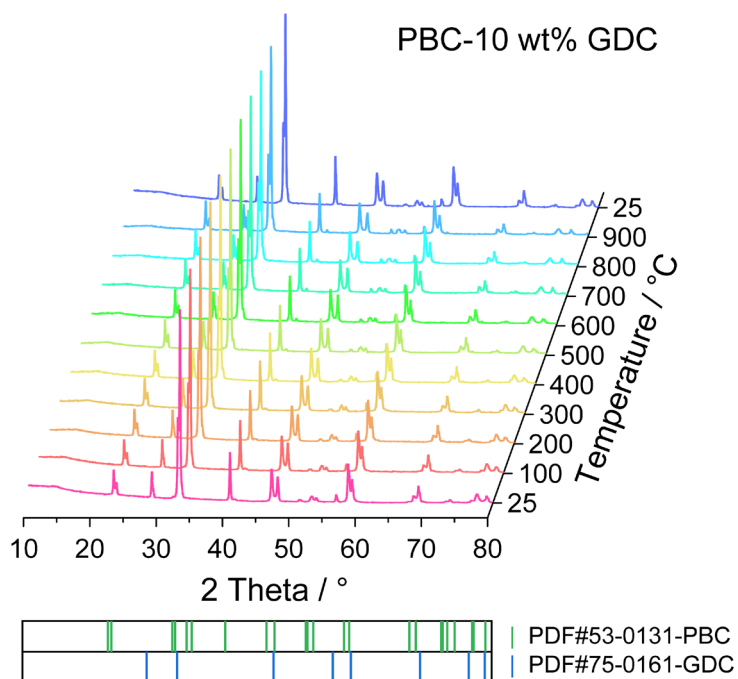Figure S2. HT-XRD patterns of PBC tested in air from RT to 900 °C and down to RT.

Figure S3. HT-XRD patterns of PBC-xGDC (x = 10 wt%) tested in air from RT to 900 °C and down to RT.

No obvious phase transformation is detected for both compounds over the heating/cooling course. The lattice parameters were derived using Rietveld refinement of the HT-XRD spectra. For all the PBC-xGDC composite samples, the tetragonal *P4/mmm* symmetry and cubic *Fm-3m* symmetry are employed for PBC and GDC, respectively.
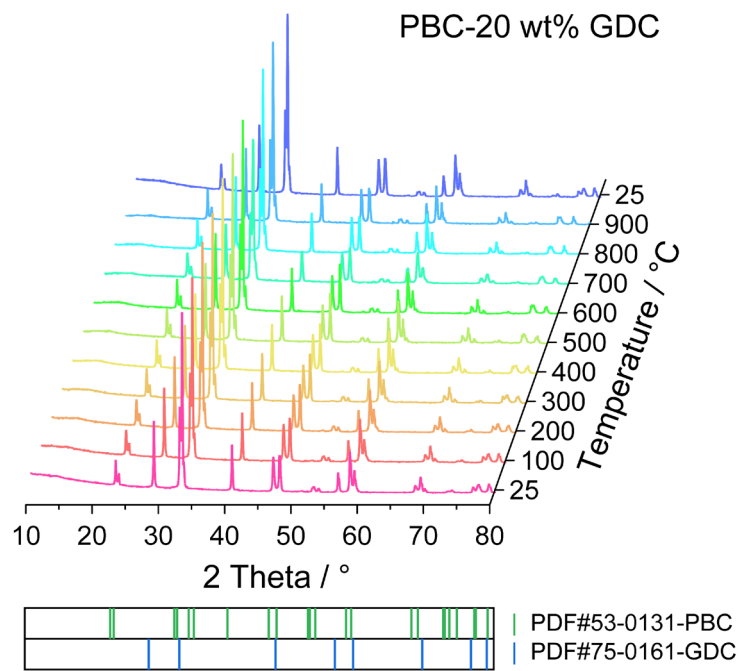
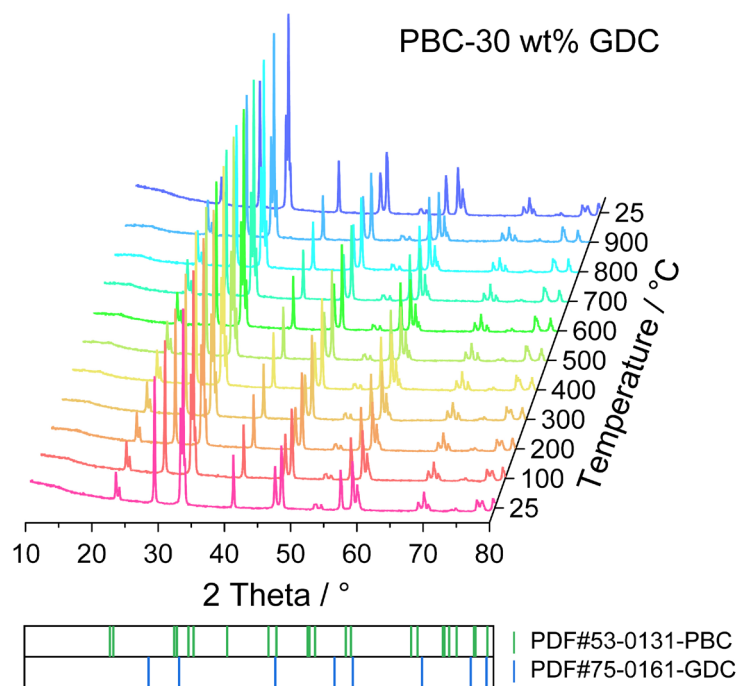Figure S4. HT-XRD patterns of PBC-xGDC (x = 20 wt%) tested in air from RT to 900 °C and down to RT.

Figure S5. HT-XRD patterns of PBC-xGDC (x = 30 wt%) tested in air from RT to 900 °C and down to RT.
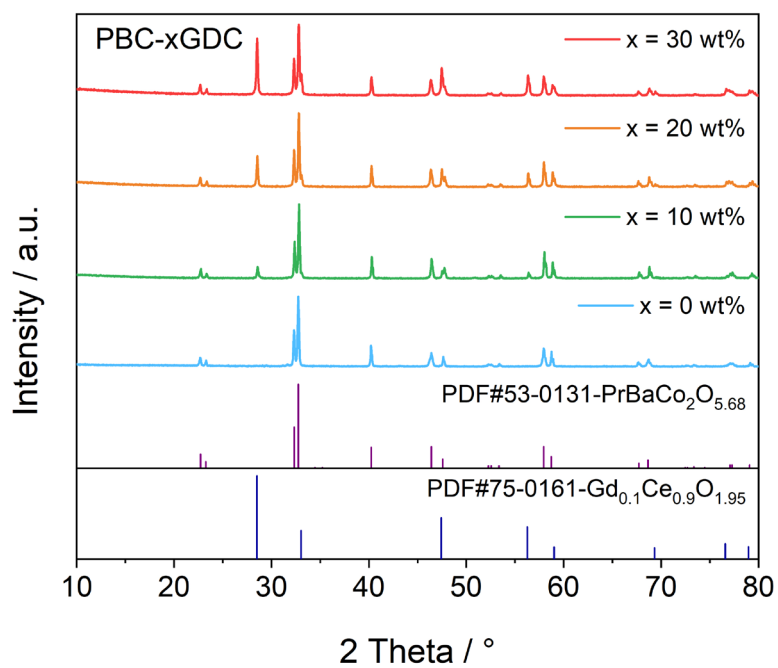
Figure S6. XRD patterns of PBC-xGDC (x = 0, 10, 20, 30 wt%) calcined at 1100 °C for 4 h.

The XRD examinations indicate that the prepared bar samples maintain good chemical stability without any impurity.
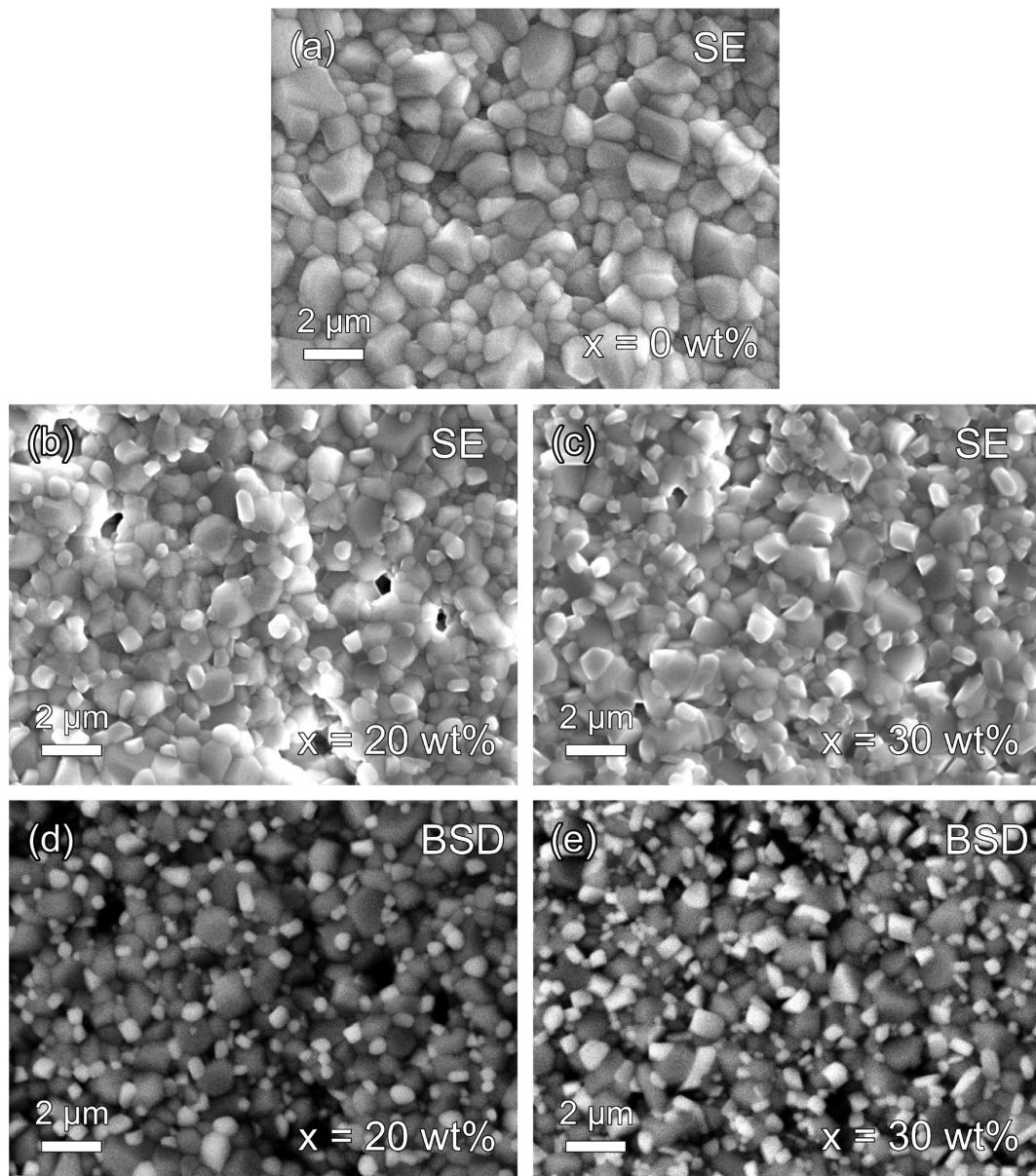
Figure S7. SEM-SE surface images (a-c) and SEM-BSD surface images (d, e) at the same location, for PBC-GDC composite bars with different amount of GDC, respectively.

PBC and GDC particles are uniformly distributed, while the GDC content has an influence on the particle size. As the quantity of GDC increases, the particle size of GDC slowly grows larger, while that of PBC decreases slightly, thus generating an extended phase boundary.
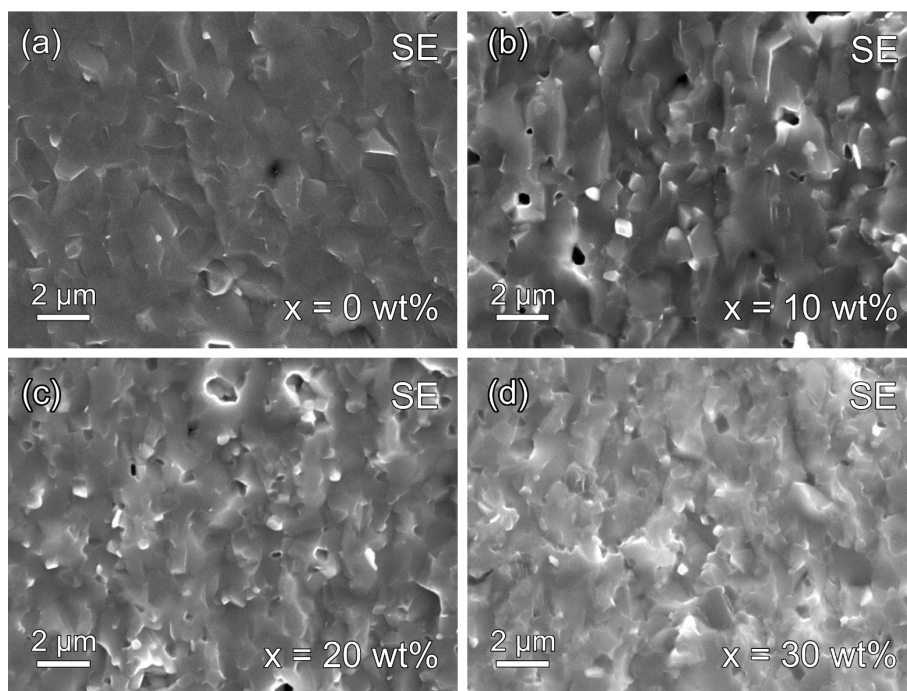
Figure S8. SEM-SE cross-section images (a-d) of PBC-xGDC (x=0, 10, 20, 30 wt%), respectively.
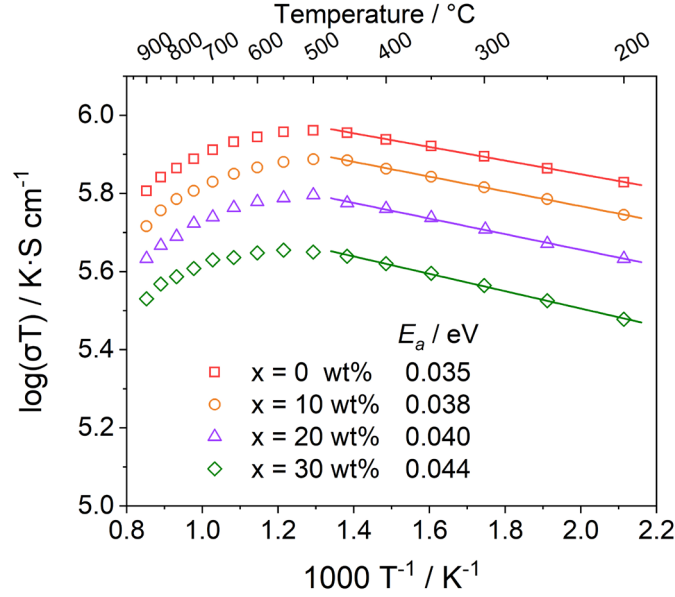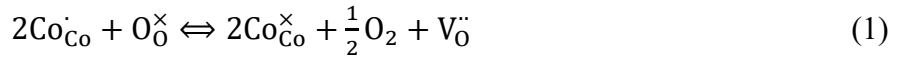
Figure S9. Arrhenius plot for PBC-xGDC (x = 0, 10, 20 and 30 wt%) electrical conductivity measured in air.

The charge carriers (electronic holes) decrease on account of the release of lattice oxygen at high temperatures. This can be explained by considering the following defect chemistry equation (1) using the Kroger-Vink notations as:

$$2Co_{Co}^{·} + O_O^{×} \Leftrightarrow 2Co_{Co}^{×} + \frac{1}{2}O_2 + V_O^{··} \tag{1}$$

where the positive charge carrier $Co_{Co}^{·}$ and the neutrally effective charged $Co_{Co}^{×}$ are the Co^{4+} ion and Co^{3+} ion at the cobalt site, respectively, and the positive oxygen vacancy is denoted as $V_O^{··}$. In the equation, the reduction of Co^{4+} at the cost of the lattice oxygen produces Co^{3+}, molecular oxygen and oxygen vacancy with the double positively effective charge. At high temperatures, the lattice oxygen in PBC phase escapes resulting in a decrease in the number of p-type electronic charge carriers, which change the conductivity behavior of the PBC phase with small polarons as the conduction mechanism. The activation energy (E_a) of the pure PBC sample is 0.035 eV.
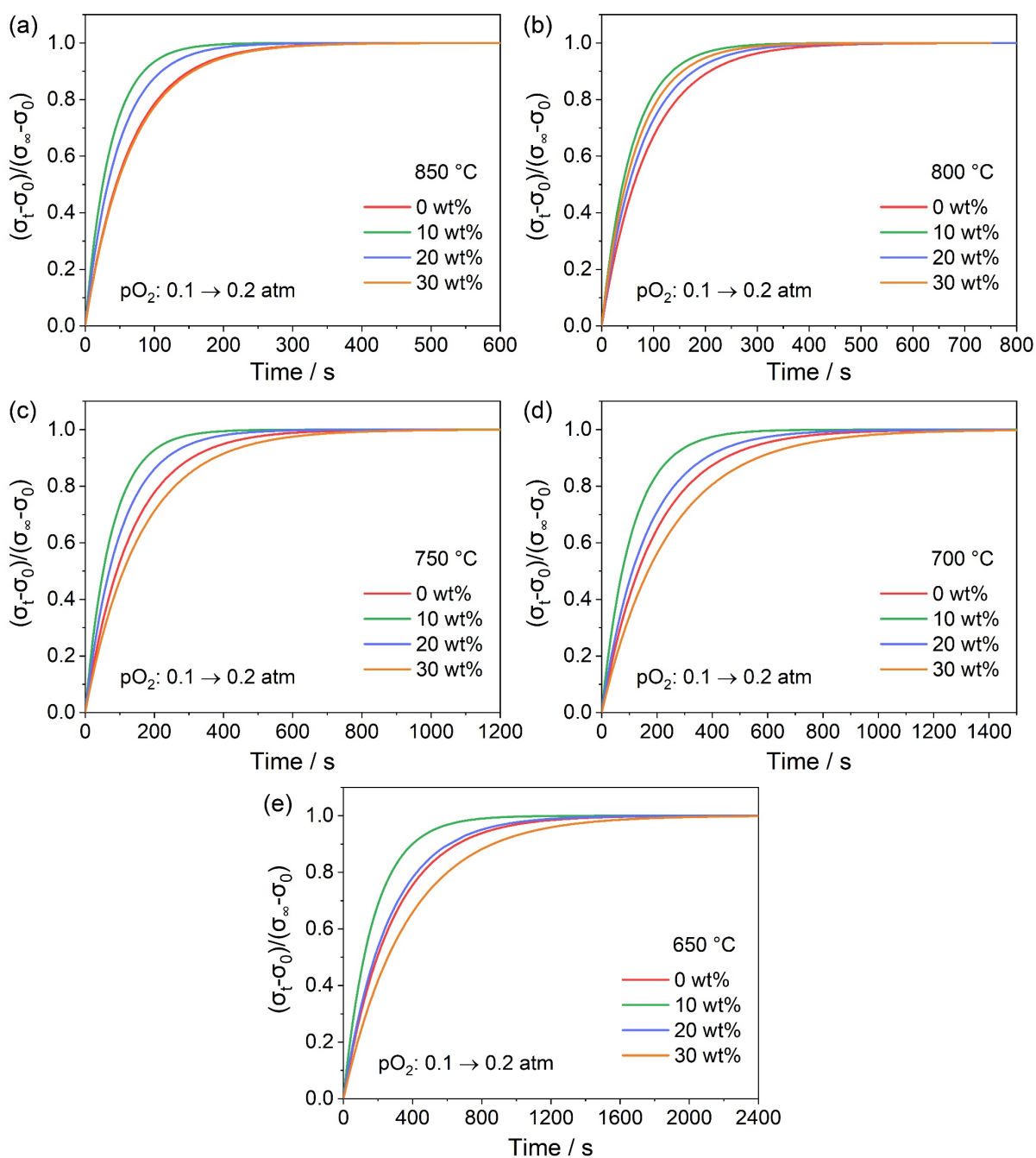
Figure S10. Normalized conductivities of PBC-GDC composites with different GDC mass fraction at (a) 850 °C, (b) 800 °C, (c) 750 °C, (d) 700 °C and (e) 650 °C.
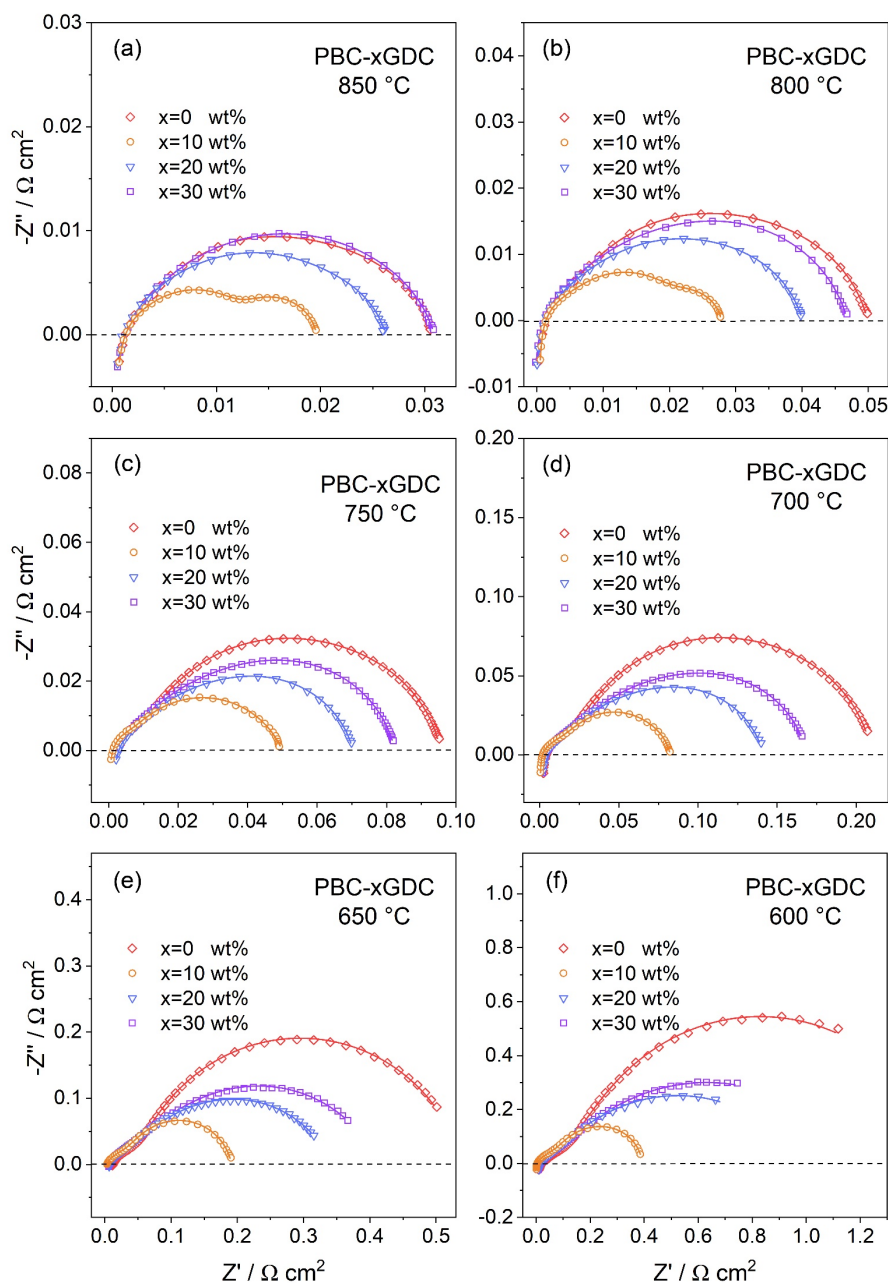
Figure S11. EIS of PBC-GDC composite electrode with various GDC contents tested in air, at (a) 850 °C, (b) 750 °C and (c) 650 °C. The scatters are original data, and the lines are fitting data.

The ohmic resistance R_o, which corresponds to the intercepts with the real axis at high frequency, mainly comes from the electrolyte. The intercept of whole arcs with the real axis belongs to the polarization resistance (R_p). The recorded R_o is normalized to zero for a clear comparison of the polarization resistance from different PBC-GDC samples.
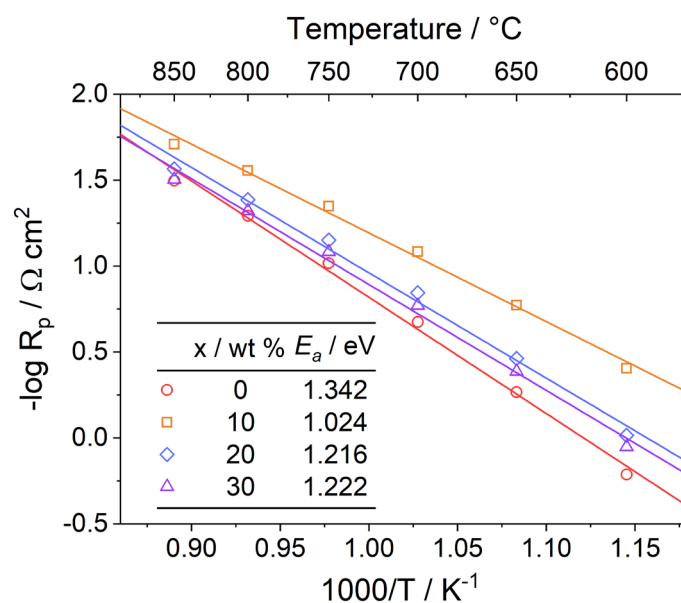
Figure S12. Arrhenius plot of polarization resistance of PBC-GDC composite electrodes with different GDC contents.

The derived E_a of the bare PBC sample is 1.342 eV, while that of x = 10, 20 and 30 wt% samples reduced to 1.024, 1.216 and 1.222 eV, respectively. Compared with the PBC, the E_a goes down when GDC exists, which indicated that the presence of GDC can provide an extra electrocatalytic activity site for the oxygen reduction, *e.g.,* PBC-GDC-gas TPB, especially in PBC-10 wt% GDC sample.
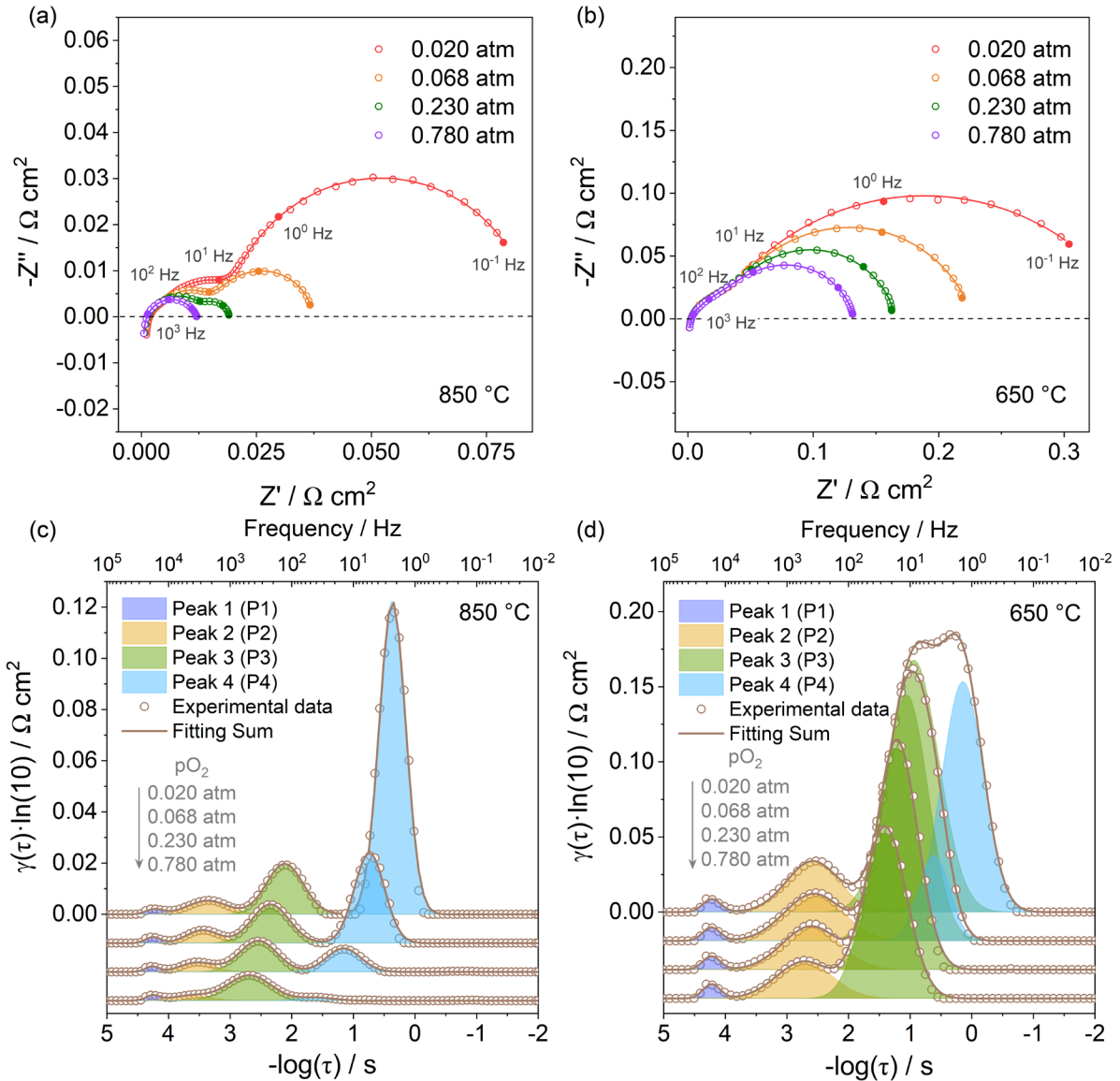
Figure S13. Nyquist plots of a symmetrical cell with PBC-10 wt% GDC electrode measured under different oxygen partial pressures, at (a) 850 °C, (b) 750 °C and (c) 650 °C, respectively.

The integral area of P1 becomes larger with the temperature reduction but is independent to oxygen partial pressure. The integral area of P2 and P3 decreases slowly with an increase in oxygen partial pressure. As the temperature decreases, the P3 and P4 gradually overlap, which seems difficult to distinguish. P4 is highly hypersensitive to oxygen partial pressure, which is almost invisible at high oxygen partial pressure, but it has less to do with the temperature.
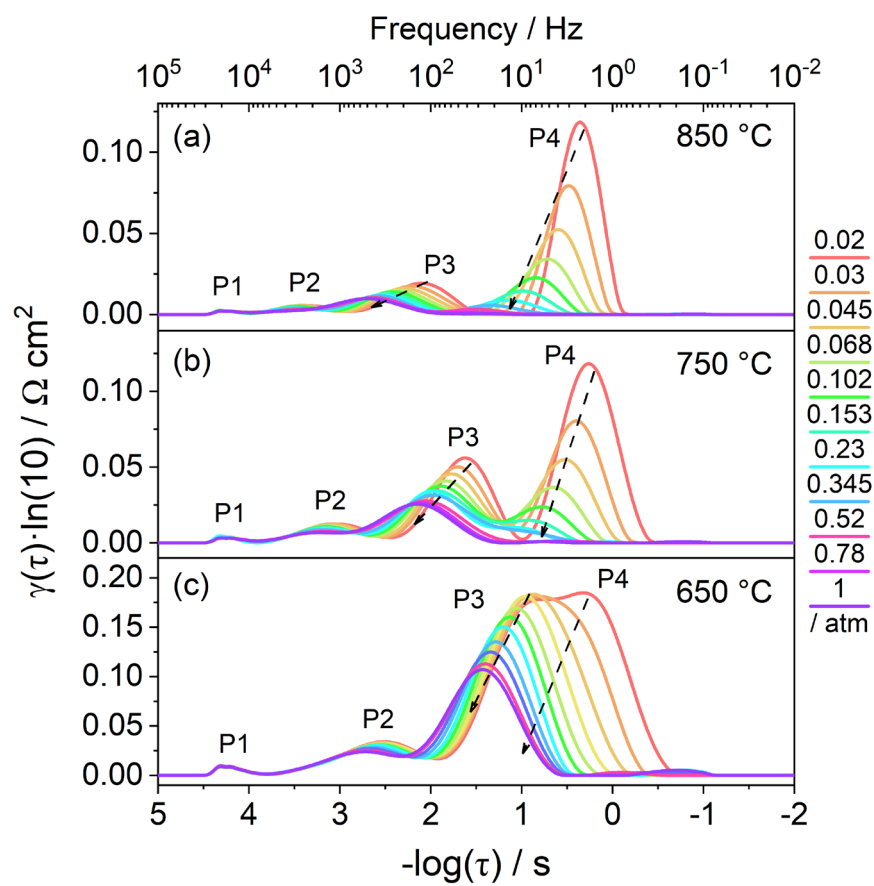
Figure S14. Series of DRT spectra at different oxygen partial pressures and temperatures of (a) 850 °C, (b) 750 °C, (c) 650 °C.
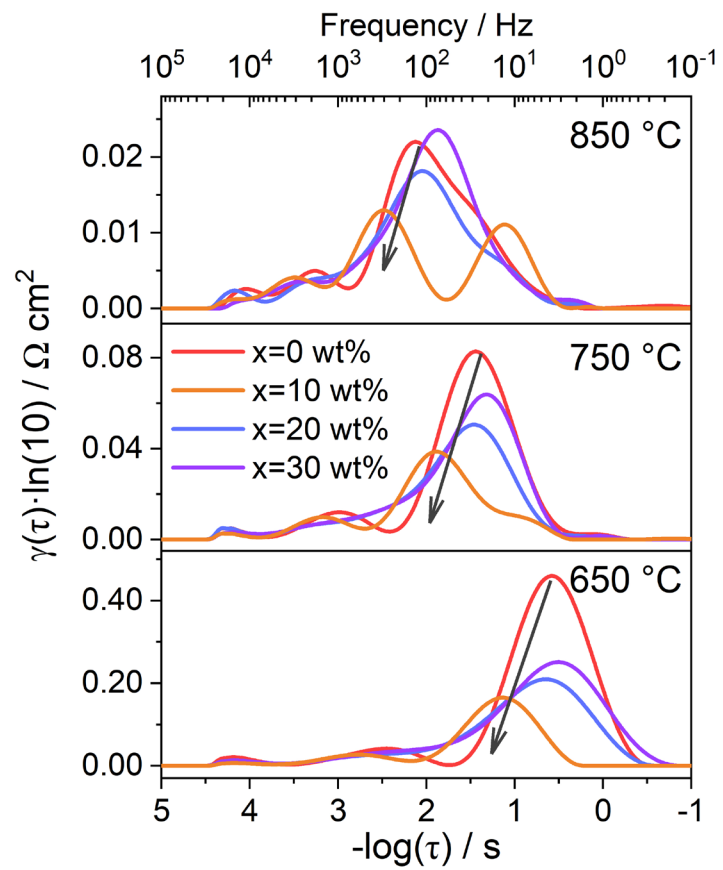
Fig. S15. DRT spectra of PBC-xGDC (x = 0, 10, 20 and 30 wt%) composite electrode measured in air.
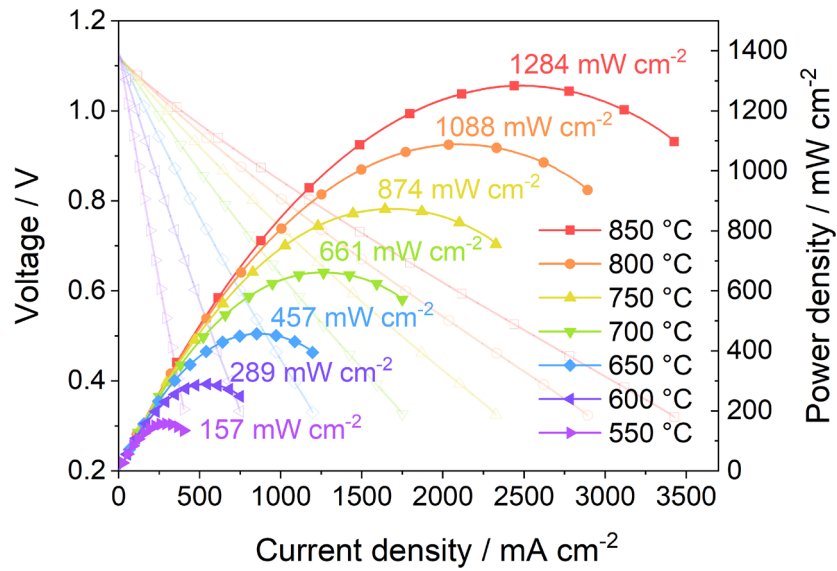
Figure S16. *I−V* and power density curves of electrolyte (LSGM, 300 μm) - supported cell with pure PBC as cathode at different temperatures fed with humidified H_2.

Because the pure PBC-10 wt% GDC has a small R_p with a low activation energy for electrode reaction, it has finite room for enhancement of electrochemical performance at high temperature, *e.g.,* 750-850 °C. Therefore, there is small difference in maximum power density for the cell of pure PBC and PBC-10 wt% GDC cathodes.

Table S1. Partial *d*-spacings of PBC and GDC phase in PBC-10 wt% GDC sample derived from Refinement data.

hkl	d / nm
PBC phase	
(001)	0.763
(100)	0.389
(002)	0.382
(101)	0.347
(110)	0.276
(102)	0.273
(111)	0.259
(003)	0.255
(112)	0.223
(103)	0.213
(200)	0.195
(004)	0.191
(201)	0.189
(113)	0.187
GDC phase	
(111)	0.312
(200)	0.270
(220)	0.191
(331)	0.163

Table S2. Polarization resistance of PBC-xGDC composite electrode with different GDC mass fraction at different temperatures. Polarization resistance units: Ω cm^2.

Temperature / °C	0 wt%	10 wt%	20 wt%	30 wt%
850	0.0318	0.0196	0.0273	0.0314
800	0.0510	0.0278	0.0411	0.0478
750	0.0961	0.0449	0.0706	0.0825
700	0.2116	0.0825	0.1429	0.1698
650	0.5407	0.1690	0.3447	0.4101
600	1.6317	0.3938	0.9669	1.1253

Table S3. Resistance of single cell with PBC-10 wt% GDC and PBC cathode at different temperatures.

Temperature / °C	PBC-10 wt% GDC		PBC	
	R_o /Ω cm^2	R_p /Ω cm^2	R_o /Ω cm^2	R_p /Ω cm^2
850	0.165	0.131	0.174	0.167
800	0.191	0.138	0.209	0.178
750	0.228	0.154	0.261	0.191
700	0.287	0.182	0.346	0.224
650	0.388	0.241	0.500	0.290
600	0.562	0.345	0.789	0.414
550	0.902	0.550	1.461	0.698